LA-UR-18-20168
Approved for public release; distribution is unlimited.

Title: A series approximation model for optical light transport and output intensity field distribution in large aspect ratio cylindrical scintillation crystals

Author(s): Tobias, Benjamin John

Intended for: Report

Issued: 2018-01-09

A series approximation model for optical light transport and output intensity field distribution in large aspect ratio cylindrical scintillation crystals

Benjamin John Tobias
Los Alamos National Laboratory
P-21 Applied Modern Physics

A series approximation has been derived for the transport of optical photons within a cylindrically symmetric light pipe and applied to the task of evaluating both the origin and angular distribution of light reaching the output plane. This analytic expression finds particular utility in first-pass photonic design applications since it may be evaluated at a very modest computational cost and is readily parameterized for relevant design constraints. It has been applied toward quantitative exploration of various scintillation crystal preparations and their impact on both quantum efficiency and noise, reproducing sensible dependencies and providing physical justification for certain gamma ray camera design choices.

INTRODUCTION

Efficient conversion of gamma- and/or x-ray photons to visible light for detection by charge-coupled devices is an important element of radiographic imaging in many medical, industrial, and scientific research applications. In lens-coupled gamma-ray cameras of the type employed for nuclear research at DARHT and the proposed ECSE facilities, this conversion is performed by a scintillating crystal that intercepts the high-energy photon flux. (For an adequate review of scintillation detector physics see [Nikl 2006].) Quantum efficiency, i.e. gain, is increased by making the crystal thicker so as to absorb more photon energy, but in a monolithic scintillation crystal this comes at a great expense in modulation transfer function, i.e. image resolution. This can be compensated by segmenting the scintillator crystal in an opaque and/or reflecting septal material. However, introduction of the septal walls and modification of the crystal geometry impact energy deposition, optical transport, and lens coupling in a variety of ways, making it sometimes complicated to predict the overall effect on imaging figures of merit such as the frequency-dependent detective quantum efficiency (DQE) [Swank 1970, Siewerdsen 2002, Gagne 2003]. These effects have been observed in experimental characterization of scintillation detectors [Cherry 1995, Globus 1997, Siewerdsen 1998, Watson 1998, Heinrichs 2002], and comprehensive explorations using Monte Carlo techniques have been carried out for some scintillator designs [Liu 2014, Roncali 2017]. However, as a foundation for understanding design trade-offs and as a first-pass design tool, analytic models are often most valuable. When they adequately represent the physical system, they most readily provide insight into parametric dependencies. For example, [Shurcliff 1949] provides a simple geometric analysis that adequately describes the trapping of light within highly symmetrical crystals and reveals simple guidelines as a function of crystal geometry and index of refraction. [Keil 1970] goes further by analyzing the properties of reflective surface preparations and their impact upon light output. Both models provide a resource for intuitive design principles. This report presents an equally simple analytical model from which to draw equally foundational design principles.

This brief report describes a simple analytic formula for obtaining the origin and angular distribution of light that may appear at the output plane of a highly symmetric scintillation crystal.

The model begins by assuming un-polarized, isotropic scintillation of incident gamma-ray energy along the axis of a high aspect ratio cylindrical crystal. The unit sphere of optical photon emission is then divided into forward and backward directed solid angles with the intensity in each zone represented by an attenuating and reflecting bundle of rays. Forward directed rays arrive at the optical output plane of the crystal, and backward directed rays are reflected or absorbed by a smooth or diffuse boundary at the upstream end of the crystal before being converted into forward directed rays. Realistic attenuation of the optical intensity within the crystal, Fresnel reflection at the sides of the crystal, and even frustrated total internal reflection (FTIR) are easily included. The resulting series equation is simple to evaluate numerically, and although it neglects diffusion of the optical ray and cannot easily accommodate a diffuse reflector at the crystal sides [Roncali 2013, 2017], it provides a simple means by which to estimate the optical Swank factor and intensity distribution as a function of crystal length for many scenarios of relevance to gamma ray camera design. In a more general sense, it can be recognized as a useful and compact expression for a variety of photonic design tasks and general ballistic transport problems.

FORWARD DIRECTED PHOTON FLUX

We begin by assuming that an isotropic flux of optical photons is produced along the axis of a cylindrical pipe with radius ρ. If we consider only the photons produced at a distance *l* from the optical output end of the pipe, then the fraction of the photon intensity that is directed toward that plane without making any reflection is,

$$\frac{\Phi_{direct}}{\Phi_0} = \frac{\int_0^{\arctan\frac{\rho}{l}} \int_0^{2\pi} r^2 \sin\theta \, d\theta d\phi}{4\pi r^2}. \tag{1}$$

If we now consider those photons that strike a wall of the light-pipe and make a single reflection, we find that they are all contained within the integral,

$$\Phi_{single\ reflection} = \int_{\arctan\frac{\rho}{l}}^{\arctan\frac{3\rho}{l}} \int_0^{2\pi} (1-\alpha) r^2 \sin\theta \, d\theta d\phi, \tag{2}$$

where α represents absorption at the reflection site. This is illustrated in Figure 1 below. Note that photons making the largest possible angle with the axis of the crystal, yet making exactly one reflection, strike the wall first at 1/3rd of their way to the output plane. Likewise, photons making exactly two reflections are encompassed by,

$$\Phi_{two\ reflections} = \int_{\arctan\frac{3\rho}{l}}^{\arctan\frac{5\rho}{l}} \int_0^{2\pi} (1-\alpha)^2 r^2 \sin\theta \, d\theta d\phi. \tag{3}$$

When all integrals of this type are included, the result is the following series:

$$\Phi_{out} = \frac{\int_0^{\arctan\frac{\rho}{l}} \int_0^{2\pi} r^2 \sin\theta \, d\theta d\phi}{4\pi r^2} + \sum_{k=1}^{\infty} \frac{\int_{\arctan\frac{(2k-1)\rho}{l}}^{\arctan\frac{(2k+1)\rho}{l}} \int_0^{2\pi} (1-\alpha)^k r^2 \sin\theta \, d\theta d\phi}{4\pi r^2}. \tag{4}$$

Evaluating the integrals, this becomes,

$$\Phi_{out} = \frac{1}{2}\left[1 - \frac{l}{\sqrt{l^2-\rho^2}} + \sum_{k=0}^{\infty}(1-\alpha)^k\left(\frac{l}{\sqrt{(2k-1)^2\rho^2+l^2}} - \frac{l}{\sqrt{(2k+1)^2\rho^2+l^2}}\right)\right]. \quad (5)$$

In this form, it becomes apparent that the series converges rather quickly. Note also that the integer k has a distinct physical meaning: it represents the number of reflections encountered by rays included in that term.

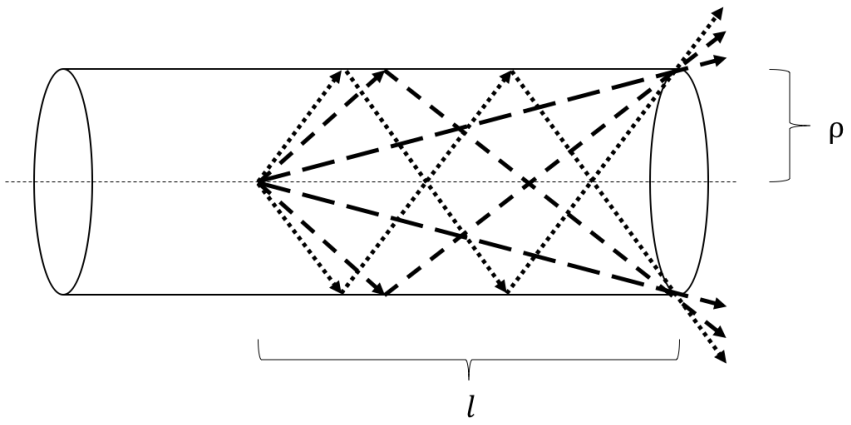

Figure 1. *Illustration of the longest rays making zero wall reflections, the longest rays making one reflection, and the longest rays making two reflections between their origin and the optical output plane of the crystal.*

An attenuation coefficient may be introduced by recognizing that the path length for an individual ray is $l/\cos\theta$. Given an attenuation coefficient β, Equation (4) becomes,

$$\Phi_{out} = \frac{1}{2}\left[\int_0^{\arctan\frac{\rho}{l}} e^{-\beta l/\cos\theta}\sin\theta\, d\theta + \sum_{k=1}^{\infty}\int_{\arctan\frac{(2k-1)\rho}{l}}^{\arctan\frac{(2k+1)\rho}{l}}(1-\alpha)^k e^{-\beta l/\cos\theta}\sin\theta\, d\theta\right]. \quad (6)$$

An approximation for this attenuation coefficient in LSO can be found in [Kriplani, 2003].

At a conducting boundary, the reflection coefficient may be taken to be,

$$R = \frac{1}{2}[R_{TE} + R_{TM}] = 1 - \left(\frac{8\epsilon_0\omega}{\sigma}\right)^{\frac{1}{2}} \equiv 1 - \alpha. \quad (7)$$

For a high-quality aluminum coating, the reflection coefficient may be as high as 0.924 at 400 nm with a skin depth of only 2.5 nm [Hass and Waylonis 1961]. At a dielectric interface, the well-known transverse-electric and transverse-magnetic Fresnel reflection coefficients (R_{TE} and R_{TM}, respectively) are given by,

$$R_{TE} = \left[\frac{n_1 \cos\left(\frac{\pi}{2}-\theta\right) - n_2\sqrt{1-\left(\frac{n_1}{n_2}\sin\left(\frac{\pi}{2}-\theta\right)\right)^2}}{n_1 \cos\left(\frac{\pi}{2}-\theta\right) + n_2\sqrt{1-\left(\frac{n_1}{n_2}\sin\left(\frac{\pi}{2}-\theta\right)\right)^2}}\right], \quad (8)$$

and,

$$R_{TM} = \left[\frac{n_1\sqrt{1-\left(\frac{n_1}{n_2}\sin\left(\frac{\pi}{2}-\theta\right)\right)^2} - n_2 \cos\left(\frac{\pi}{2}-\theta\right)}{n_1\sqrt{1-\left(\frac{n_1}{n_2}\sin\left(\frac{\pi}{2}-\theta\right)\right)^2} + n_2 \cos\left(\frac{\pi}{2}-\theta\right)}\right]. \quad (9)$$

Dielectric interfaces produce total internal reflection (TIR) at an incident angle smaller than the well-known critical angle. Therefore, there appears a critical integer, k_c, which represents the number of reflections experienced by a ray at an angle infinitesimally smaller than the critical angle for TIR. This integer is the smallest integer greater than,

$$\frac{1}{2}\left[\tan\left(\frac{\pi}{2} - \arcsin\frac{n_2}{n_1}\right)\frac{l}{\rho} - 1\right]. \quad (10)$$

The TIR effect allows the summation to be simplified in the following form,

$$\Phi_{out} = \frac{1}{2}\left[\int_0^{\frac{\pi}{2}-\arcsin\frac{n_2}{n_1}} e^{-\beta l/\cos\theta}\sin\theta\, d\theta + \int_{\frac{\pi}{2}-\arcsin\frac{n_2}{n_1}}^{\arctan\frac{(2k_c+1)\rho}{l}} R^{k_c} e^{-\beta l/\cos\theta}\sin\theta\, d\theta + \sum_{k=k_c+1}^{\infty}\int_{\arctan\frac{(2k-1)\rho}{l}}^{\arctan\frac{(2k+1)\rho}{l}} R^k e^{-\beta l/\cos\theta}\sin\theta\, d\theta\right], \quad (11)$$

which requires fewer evaluations of the Fresnel reflection coefficients. The first term in this expression is easily modified to accommodate losses from the FTIR effect when it is appropriate. Furthermore, it reveals that the largest contribution to the light output comes from so-called TIR light in many practical cases. Figure 2, part a, shows the relative contributions to forward directed flux arriving at the optical output plane for crystals with high-quality aluminum and quartz (SiO2) reflective coatings. These calculations neglect the problem of coupling light out of the crystal and into the detector, but nonetheless reveal that much more light is available for output coupling when a TIR reflection is provided along the sides of a high aspect ratio crystal. Only for crystals shorter than 2 cm (aspect ratio < 200) does a high-quality Al coating provide any benefit. (Coincidentally, this additional intensity is at large angles to the output plane.) Part b of Figure 2 shows that optimization of the TIR critical angle provides a benefit for crystals of all lengths. The most important caveats here are the feasibility of completely surrounding a crystal in air, and the potential tradeoffs that would be observed when gamma-ray energy deposition were taken into account. Neither undermines the importance or validity of the design principle that is implied.

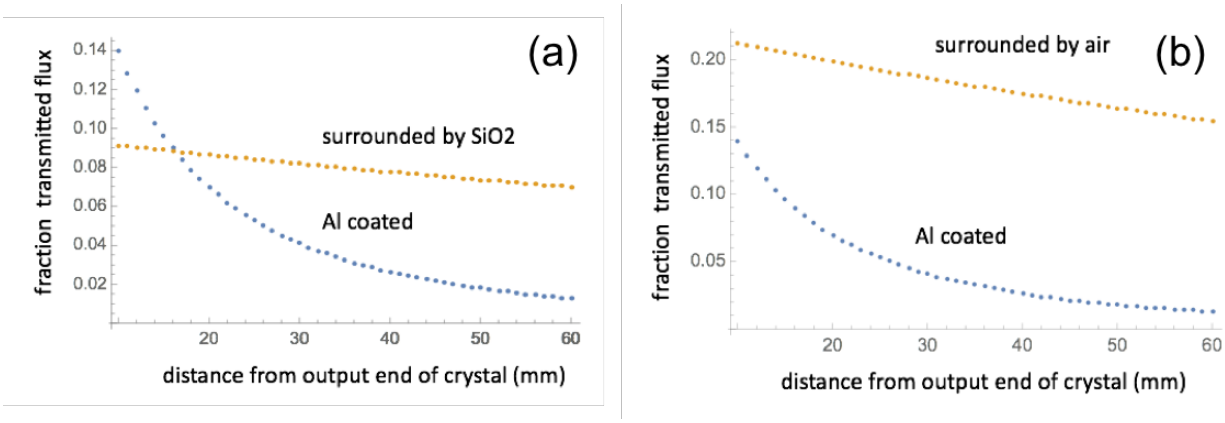

Figure 2. *a) The normalized fraction of scintillation photon flux arriving at the output plane of a cylindrical crystal vs. the distance from the output end at which the photon is generated for an LSO crystal (n=1.82, ρ =0.505 mm, β =0.0048 mm^{-1}) surrounded by either Al (R=0.924) and SiO2 (n=1.47). b) The same crystal surrounded by either Al or dry Air (n=1.0).*

BACKWARD DIRECTED PHOTON FLUX

The additional contribution from photons that are initially directed toward the gamma-ray incident end of the crystal is easily accounted for. By defining the overall length of the crystal, z, Equation (11) can be used to compute the photon flux arriving at the upstream plane simply by substituting $l \to z - l$. For a dielectric boundary (or an interface with air), the Fresnel coefficient must be evaluated before propagating the ray back toward the output end of the crystal. For a very smooth reflecting conductor, the reflectivity of the conductor is taken from the appropriate references as a function of angle. In either case, this flux is accounted for by simple modifications of (11). A slightly more sophisticated approach should be adopted for diffuse reflectors, the simplest model being a Lambertian distribution [Keil 1970]. This, for example, might be adopted in an equation of the form,

$$\Phi_{out}^{back} = \frac{1}{2}\left[\int_0^{\frac{\pi}{2}-\arcsin\frac{n_2}{n_1}} e^{-\beta(2z-l)/\cos\theta} R_b \cos\theta \sin\theta \, d\theta + \right.$$
$$\int_{\frac{\pi}{2}-\arcsin\frac{n_2}{n_1}}^{\arctan\frac{(2k_c+1)\rho}{l}} R^{k_c} e^{-\beta(2z-l)/\cos\theta} R_b \cos\theta \sin\theta \, d\theta +$$
$$\left.\sum_{k=k_c+1}^{\infty} \int_{\arctan\frac{(2k-1)\rho}{l}}^{\arctan\frac{(2k+1)\rho}{l}} R^k e^{-\beta(2z-l)/\cos\theta} R_b \cos\theta \sin\theta \, d\theta\right], \qquad (12)$$

where $R_b \cos\theta$ describes the conversion of the intensity to a Lambertian distribution reflecting from the back, or upstream, crystal face.

Even the best reflector cannot more than double the light output. However, it can modify the gamma ray camera's performance by altering the origin of light reaching the output end. A reflector, particularly a diffuse reflector that scatters more light to small angles with the optical axis, tends to preferentially improve transport for photons generated far from the output plane. Depending on the output coupling condition, this may improve the optical Swank factor by

enhancing the number of coupled photons generated in regions of large radiation Swank factor (narrow pulse height distribution). This is best explored in conjunction with a radiation deposition model and therefore reserved for a later report.

INTENSITY DISTRIBUTION INCIDENT AT THE OUTPUT PLANE

The form of Equation (6) readily lends itself to evaluation of the intensity distribution at the output plane, since each term represents the intensity within an annular zone of solid angle on the far-field unit sphere. In addition to the integral contained within each term, only the solid angle and mean polar angle need be calculated in order to reconstruct an approximation for the far-field intensity pattern. The resolution obtained for a given intensity distribution is determined by the limits of integration in each term, and is therefore more crude when taken for photons generated very near the output end of the crystal. This limits the utility of the method when dealing with scintillators having low aspect ratio elements. But, when evaluated for large aspect ratio applications it validates one's expectation that the intensity pattern incident on the output plane is relatively uniform across the solid angle bounded by the TIR critical angle and provides a quantitative starting point for subsequent optical coupling calculations. This is shown in Figure 3. Note that the distribution is less well defined for photons originating very near the output plane. This is due in part to loss of resolution, but also to the additional contribution of light reflecting from the scintillator walls at angles smaller than the critical angle. This light is attenuated by multiple lossy reflections when generated deeper within the crystal and makes a small contribution to the overall light output.

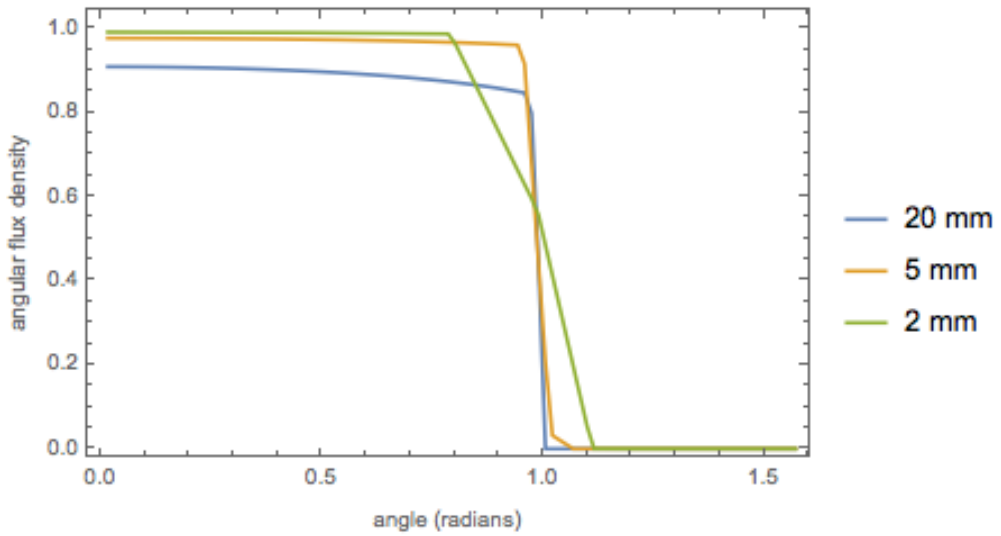

Figure 3. *The approximate far-field intensity patterns produced by light originating 2 mm, 5 mm, and 2 cm within a scintillating crystal. Note the use of linear interpolation in this plot.*

SUMMARY AND CONCLUSIONS

A straight-forward geometric approach to visible photon transport within a cylindrical scintillator crystal results in a compact series approximation for the light incident at the optical output plane that includes absorption along the ray path, reflection from conducting or dielectric boundaries,

and various types of back-reflectors. Evaluation of this series simply and intuitively demonstrates the benefit of TIR reflections at dielectric boundaries for high aspect ratio scintillator crystals, and the potential degradation in performance from finite absorption when conducting coatings are used. Simple modifications of the equation provide a path forward in evaluating the impact of various back reflectors, including Lambertian diffuse reflectors, on light output and total Swank noise performance. Finally, the equation is shown to produce the expected photon flux density at the optical output plane, an important component of quantitatively evaluating output coupling schemes. The fact that photons are produced along the axis of the crystal in this model has virtually no bearing on the validity of the result for relevant aspect ratios: a finite aperture is well-represented as a collection of sources, each having an intensity distribution identical to that obtained using the on-axis approximation.

Pertinent to first-pass design of a scintillating detector for the ECSE-Scorpius project, it has been verified that LSO crystals loosely packed in a scintillator septal frame such that their boundaries are almost entirely in contact with air can be expected to perform better than those with any other feasible preparation, such as a metallic or fluoride coating. Additionally, a back-reflector can be expected to boost optical output and preferentially enhance coupling of photons generated near the gamma-ray entrance of the scintillator. In the future, this will be explored in more detail by coupling this simple model to Monte Carlo simulations of the gamma-ray energy deposition.

REFERENCES

M. Nikl, Meas. Sci. Technol. **17**, R37 (2006).

R.K. Swank, J. Appl. Phys. **44**, 4199 (1970).

J.H. Siewerdsen, et al., Med. Phys. **29** 2655 (2002).

R.M. Gagne, et al., Med. Phys. **30**, 2180 (2003).

S.R. Cherry, et al., IEEE Trans. Nucl. Sci. **42**, 1058 (1995).

M.E. Globus, et al., IEEE Nuclear Science Symposium, Anaheim, CA, 1996

J.H. Siewerdsen, et al., Med. Phys. **25**, 614 (1998).

S.A. Watson, et al., LA-UR 98-2523

U. Heinrichs, et al., Nucl. Instrum. and Methods in Phys. Res. A **486**, 60 (2002).

L. Liu, et al., Med. Phys. **41**, 061916 (2014).

E. Roncali, et al., Phys. Med. Biol. **62**, R207 (2017).

W.A. Shurcliff and R.C. Jones, J. of the Opt. Soc. of Amer. **39**, 912 (1949).

G. Keil, Nucl. Instrum. and Methods **87**, 111 (1970).

E. Roncali and S.R. Cherry, Phys. Med. Biol. **58**, 2185 (2013)

E. Roncali, et al., Phys. Med. Biol. **62**, 4811 (2017)

A. Kriplani, et al., IEEE Nuclear Science Symposium, Portland, OR, 2003

G. Hass and J.E. Waylonis, J. of the Opt. Soc. of Amer. **51**, 719 (1961).